Global NEST Journal, Vol 27, No 1, 06931

The use of arum italicum root extracts for protection against corrosion and green synthesis of silver nanoparticles: investigation of their photocatalytic and antimicrobial properties

Zouied D.[1]*, Chettah W.[1], Khelfaoui M.[1], Bouzenad N.[2], Abdennouri A.[2], Dob K.[2], Boulehsa A.[3], Bouhali H.[4], Karima Derdour K.[1], Ammouchi N.[4] and Zouaoui E.[2]

[1]Laboratory of Chemical Engineering and Environment of Skikda (LGCES), University-20 Aout-1955-Skikda, Algeria
[3]Laboratory of interactions, biodiversity, ecosystems and biotechnology (LIBEB), University 20 august 1955 Skikda (Algeria)
[4]Laboratory of Physico-Chemical research of Surfaces and Interfaces, University 20 Août 1955, Skikda, (Algeria)
Received: 27/10/2024, Accepted: 25/11/2024, Available online: 13/12/2024
*to whom all correspondence should be addressed: e-mail: d.zouied@univ-skikda.dz
https://doi.org/10.30955/gnj.06931

Graphical abstract

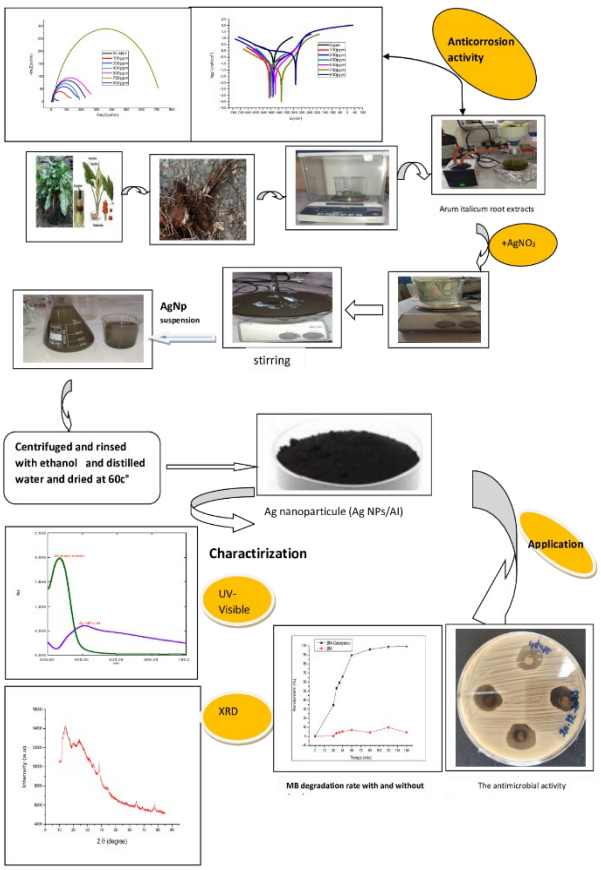

Abstract

The main objective of this work is to investigate sustainable ways to corrosion inhibition and photocatalytic applications using natural extracts and green synthesis processes. Specifically, the study investigates at the utilization of an ethanolic extract from the Arum italicum plant as a mild steel corrosion inhibitor in a 1M HCl solution. The extract demonstrated significant corrosion inhibition, with effectiveness influenced by both the concentration of the extract and the temperature of the environment. Polarization studies revealed a maximum inhibition efficiency of 97.85% at 750 ppm, which was corroborated by an efficiency of 97.21% observed through Electrochemical Impedance Spectroscopy (EIS). The results indicate that the extract acts as a mixed-type inhibitor, and its adsorption onto the steel surface follows the Langmuir isotherm, suggesting a physical adsorption mechanism. Beyond corrosion inhibition, the study also explores the green synthesis of silver nanoparticles (Ag NPs) using the Arum italicum extract. These Ag NPs showed outstanding photocatalytic activity, achieving approximately 98% degradation of methylene blue within 150 minutes under sunlight exposure, underscoring their potential for photocatalytic applications in natural light conditions. The antimicrobial efficacy of the synthesized Ag NPs was also assessed, revealing significant inhibition against *E. coli*, *S. aureus*, and *P. aeruginosa*. The Ag NPs were effective against both gram-positive and gram-negative bacteria, with larger inhibition zones observed at higher nanoparticle concentrations, confirming their broad-spectrum antimicrobial properties.

Keywords: Ag nanoparticles, antimicrobial activity, *arum italicum*, corrosion inhibition, green synthesis, mild steel, photocatalysis

1. Introduction

Nanotechnology has recently emerged as a pivotal field in creating novel materials with distinct physicochemical properties, particularly metal oxides, for a wide range of industrial, medical, and environmental applications (Kavitha *et al*. 2020; Medhi *et al*. 2020). Metal nanoparticles, including silver, gold, and zinc oxides, are renowned for their unique optical, electronic, and

catalytic properties, which have led to breakthroughs in fields such as medicine, electronics, and environmental remediation (Nair *et al*. 2022). However, conventional physical and chemical synthesis methods of nanoparticles often involve the use of hazardous solvents, high energy consumption, and toxic reagents, raising significant environmental and safety concerns (Qin *et al*., 2019). Consequently, there is a growing interest in developing greener, more sustainable approaches to nanoparticle synthesis, leveraging biological methods that are both cost-effective and eco-friendly (Rasool *et al*., 2024; Singh *et al*. 2024).

Among the biological methods, plant-mediated synthesis of nanoparticles has garnered considerable attention due to its simplicity, availability of plant resources, and the inherent stability of the produced nanoparticles (Shyam *et al*. 2021). This method utilizes plant extracts as both reducing and stabilizing agents, bypassing the need for toxic chemicals and enabling large-scale production with minimal environmental impact (Ahmed *et al*. 2022). Silver nanoparticles (Ag NPs), in particular, have found applications across numerous sectors, including alternative medicine, sensors, spectroscopy, catalysis, corrosion inhibition, antimicrobial, anticancer treatments, and agriculture, making them one of the most studied nanomaterials (Hublikar *et al*. 2021; Tehri *et al*. 2022; Harish *et al*. 2022).

The historical use of medicinal plants for healing spans centuries, deeply rooted in the traditional practices of various ancient civilizations, including Roman, Indian, Chinese, and Arab-Muslim medicine, which have extensively documented the therapeutic properties of plants in treating numerous ailments (Shikov *et al*. 2014; Barrett *et al*. 2001). These ancient systems of medicine, such as Ayurveda, Traditional Chinese Medicine (TCM), and Unani, relied on plant-based remedies for their natural availability, efficacy, and minimal side effects compared to synthetic drugs (Ahmad Khan *et al*. 2019; Bouzana *et al*. 2023). This long-standing tradition underscores the potential of medicinal plants as a sustainable resource not only for healthcare but also for modern technological applications such as nanoparticle synthesis. In recent years, the bioactive compounds derived from medicinal plants have garnered attention for their antioxidant, antimicrobial, and anticorrosive properties, which are highly desirable for the development of eco-friendly and biocompatible nanomaterials (Haneefa *et al*. 2017).

The renewed interest in plant-derived natural products as eco-friendly alternatives to conventional corrosion inhibitors addresses the growing need for green corrosion protection solutions in industries. Conventional corrosion inhibitors often involve toxic chemicals that pose environmental and health hazards, prompting a shift towards greener alternatives (Rizi *et al*., 2023). Plant extracts, rich in polyphenols, alkaloids, flavonoids, and other phytochemicals, offer effective corrosion inhibition through adsorption on metal surfaces, thereby forming protective layers that mitigate corrosion processes (Ferkous *et al*., 2023; Himeur *et al*. 2024). This approach not only aligns with sustainable development goals but also provides a cost-effective and accessible solution for corrosion protection, particularly in developing regions where industrial infrastructure may be limited (Al-Amiery *et al*. 2024).

Arum italicum, a member of the *Araceae* family, is a perennial plant native to the Mediterranean regions of North Africa, particularly Algeria, Morocco, and Tunisia (Calabrese *et al*. 2012). The plant has been traditionally used for various purposes, reflecting its versatility and importance in local cultures. Its tubers and leaves have been employed in the production of soap in Europe, while locally, they are consumed during specific times of the year to avoid their inherent toxicity (Meeuse *et al*. 1989). The plant's tubers are traditionally used for treating breast cancer, while its leaves are known for alleviating coughs, demonstrating its therapeutic potential (Meeuse *et al*. 1989; Govindaraju *et al*., 2008; Lengke *et al*. 2007). Additionally, *Arum* italicum is known for its rich composition of bioactive compounds, including saponins (Sanna *et al*. 2020), flavonoids (Rechek *et al*. 2023), and alkaloids (Kozuharova *et al*. 2023), which contribute to its medicinal properties and provide a robust platform for further exploration in nanotechnology.

Given its diverse array of bioactive compounds, Arum italicum presents an unexplored potential for the green synthesis of nanoparticles. The use of this plant in synthesizing nanoparticles, particularly silver nanoparticles (Ag NPs), could provide significant advantages in developing multifunctional nanomaterials with applications in corrosion inhibition, catalysis, and antimicrobial treatments (Imchen *et al*. 2022). This approach not only leverages the plant's natural properties but also contributes to the broader goal of sustainable nanotechnology by reducing the reliance on hazardous chemicals traditionally used in nanoparticle synthesis (Singh *et al*. 2024).

The green synthesis of nanoparticles using biological entities, such as plants, algae, bacteria, fungi, and even viruses, represents a novel, rapid, cost effective, and environmentally benign alternative to conventional methods (Haneefa *et al*. 2017). Plant extracts are particularly advantageous due to their easy accessibility, low cost, and safe handling. They act as both reducing agents, converting metal ions into nanoparticles, and stabilizing agents, preventing particle agglomeration and ensuring uniform size distribution. This dual functionality is crucial for producing nanoparticles with enhanced stability and desired properties for various applications (Medhi *et al*. 2020; Rizi *et al*., 2023; Ferkous *et al*., 2023). The incorporation of green synthesis methods not only supports environmental sustainability but also opens new avenues for the development of advanced materials that are both efficient and eco-friendly.

By exploring the green synthesis of Ag NPs using *Arum italicum* extracts, this research aims to harness the untapped potential of this plant in the context of developing multifunctional nanomaterials. The study

investigates the anti-corrosive, photocatalytic, and antimicrobial activities of the synthesized Ag NPs, highlighting their potential applications across various sectors. This pioneering work on *Arum italicum* not only advances the field of green nanotechnology but also underscores the broader applicability of medicinal plants in modern scientific innovations.

2. Materiel and methods

2.1. Collection and preparation of arum italicum root extracts

Arum italicum roots were harvested in Bin El-Ouiden, Tamalous, located west of Skikda in north eastern Algeria (latitude: 36,8082° or 36° 48' 30" N, longitude: 6,56684° ou 6° 34' 1" est E). The roots were carefully washed with distilled water and air-dried at room temperature in the dark. Once dried, the roots were ground to a fine powder, and 20 g of this powder was soaked in 400 ml of acidified ethanol at room temperature. The solution was then filtered, and the filtrate was concentrated using a rotary evaporator at reduced pressure to remove the solvent efficiently. The concentrated extract was further dried at 35°C and stored in a laboratory cabinet at room temperature for future use (**Figure 1**).

Figure 1. Overview of sampling site

2.2. Preparation of Silver Nanoparticles

Silver nanoparticles (Ag NPs) were synthesized using a green method with *Arum italicum* root extract, following a modified procedure from previous studies (Zouied *et al*. 2022). Initially, the root extract was prepared at a concentration of 1000 ppm. For the synthesis, A 1000ppm solution of silver nitrate (AgNO3) was prepared, and 1000 ml of this solution was added to500 ml of the extract under continuous stirring. The reaction mixture was maintained at a temperature of 25–30°C with constant stirring, and the addition of $AgNO_3$ led to a gradual color change, indicating the formation of silver nanoparticles. The resulting nanoparticles were then washed three times with distilled water to remove any residual ions. Following purification, the nanoparticles were oven-dried at 35°C for 24 hours. Finally, the dried nanoparticles were stored in an amber-colored reagent bottle at room temperature for further analysis.

2.2.1. Characterization of arum italicum extract and synthesized Ag NPs/AI

The Arum italicum extract and synthesized silver nanoparticles (Ag NPs/AI) were characterized using UV-Visible spectroscopy and X-ray diffraction (XRD). UV-Vis spectroscopy was used to analyze the absorbance spectra within the 200–800 nm range, while XRD analysis was conducted using Cu-Kα radiation to determine the crystalline structure of the nanoparticles.

2.3. Preparation of electrodes and electrolytic medium

The experiments utilized carbon steel (Fe-C) electrodes, with the following chemical composition: Titanium (Ti) 0.04%, Iron (Fe) 94.66%, Manganese (Mn) 0.3%, Chromium (Cr) 0.03%, Molybdenum (Mo) 0.03%, Vanadium (V) 0.03%, and Nickel (Ni) 0.18%. The working electrode was embedded in epoxy resin, exposing a surface area of approximately 1 cm^2. Prior to use, the electrode surface was carefully prepared by sequential polishing with emery papers of decreasing grit sizes (1200 to 250 grit) to achieve a smooth and uniform finish, followed by degreasing with acetone to eliminate any residual contaminants. The electrolytic medium employed in the experiments was a 1M hydrochloric acid (HCl) solution.

2.4. Electrochemical methods

Electrochemical studies were conducted using a three-electrode cell configuration, comprising carbon steel as the working electrode, a platinum electrode as the counter electrode, and a saturated calomel electrode as the reference electrode. Polarization and electrochemical impedance spectroscopy (EIS) experiments were performed using a Voltalab PGZ 301 potentiostat/galvanostat system. The polarization experiments were conducted at a scan rate of 10 mV/s, with a potential range from -1200 to -200 mV. Impedance (Z) and phase shift (θ) measurements were recorded over a frequency range of 100 kHz to 100 MHz.

$$E(\%) = \frac{\mathrm{Rct} - \mathrm{R°ct}}{Rct} \times 100 \quad (1)$$

Where R_{ct} and R^0_{ct} are the charge transfer resistances in the presence and absence of inhibitor, respectively. Electrochemical parameters such as the corrosion potential (Ecorr), corrosion current (Icorr), and anodic (ba) and cathodic (bc) Tafel slopes were obtained, and the inhibition efficiency was calculated using,

$$E(\%) = \frac{(I°corr - Icorr)}{I°corr} \times 100 \quad (2)$$

Where $I°_{corr}$ and I_{corr} are the corrosion current densities without and with the inhibitor, respectively (Zouied *et al*. 2022; Behpour *et al*. 2008).

2.5. Photocatalytic activity

The photocatalytic activity of the synthesized silver nanoparticles was evaluated by monitoring the degradation of methylene blue (MB) dye. The initial concentration of the MB solution was 7.5 ppm. A 0.2 g sample of the photocatalyst was added to 200 ml of the MB solution, and the degradation process was initiated under sunlight irradiation. The concentration of MB in the irradiated solution was measured at regular intervals using UV-Vis spectroscopy (Shimadzu 1800) at a wavelength of 664 nm.

2.6. Antimicrobial activity

The antimicrobial efficacy of the synthesized silver nanoparticles (Ag NPs) from Arum italicum was evaluated following protocols adapted from previous studies (Ouali *et al*. 2010; Bouzenad *et al*. 2024). The activity was tested against bacterial strains from the American Type Culture Collection (ATCC), including *Staphylococcus aureus* ATCC® 6538 (gram-positive), *Escherichia coli* ATCC® 25922, and *Pseudomonas aeruginosa* ATCC® 27853 (both gram-negative). An agar diffusion test was employed to assess bacterial growth inhibition. Each bacterial strain was cultured in nutrient broth for 18 hours at 37°C, and the bacterial inoculums were prepared aseptically, with cell density adjusted to 10^6 CFU/mL. The synthesized silver nanoparticles were serially diluted, and 30 µL of each dilution was applied to discs placed on agar plates. After 24 hours of incubation at 37°C, the inhibition zones were measured to determine the antimicrobial activity.

3. Results and discussion

3.1. Characterization of Arum italicum Extract and Synthesized Ag NPs/Al

The UV-Vis spectra of the Arum italicum plant extract and the synthesized Ag NPs/Al were analyzed to assess the reduction of silver ions. As shown in **Figure 2** the spectrum of the plant extract displayed a peak at 333.5 nm, indicating the presence of bioactive compounds, while the Ag NPs/Al exhibited a marked decrease in signal intensity around 406.5 nm and a complete disappearance of the peak at 670 nm, which confirms the reduction of Ag+ ions to metallic silver (Bouzenad *et al*. 2024; Imchen *et al*. 2022).

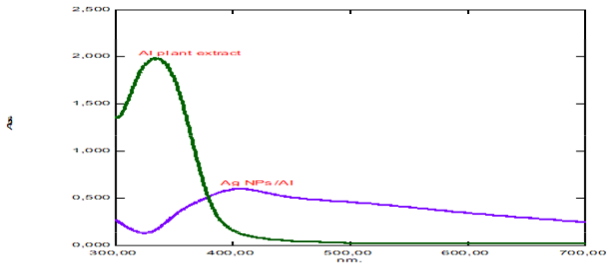

Figure 2. UV-vis spectra of Al plant extract and Ag NPs/Al

To better characterize the produced nanoparticles, X-ray diffraction (XRD) examination was used. The XRD pattern revealed peaks at 2θ values of 37°, 48°, 67°, and 78°, corresponding to the (111), (200), (220), and (301) lattice planes of the face-centered cubic structure of Ag NPs. These diffraction peaks, displayed in **Figure 3**, align with reference data, confirming the crystalline structure of the synthesized Ag NPs (Liu *et al*. 2018).

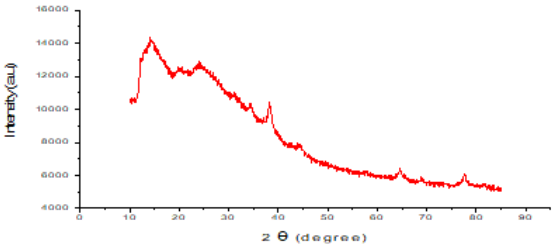

Figure 3. XRD pattern of Ag Nps/Al.

3.2. Assessment of Anticorrosion Properties of Arum italicum Root Extract

3.2.1. Polarization curves

The polarization curves for carbon steel (Fe-C) immersed in a 1M HCl solution, with and without varying concentrations of Arum italicum extract at 25°C, are shown in **Figure 4**.

When plotting log I against E, the curves display two distinct regions: a cathodic section corresponding to the reduction of oxygen on the steel surface and an anodic section associated with the oxidation reaction. Key parameters, including corrosion current density (Icorr), corrosion potential (Ecorr), cathodic and anodic Tafel slopes (Bc and Ba), inhibition efficiency (E%), and surface coverage (θ) for different extract concentrations, are summarized in **Table 1**. The inhibition efficiency (E%) is calculated using Equation (1).

The data presented in **Table 1** show a clear trend in which the corrosion current densities (Icorr) decrease as the concentration of the extract increases, reaching a maximum inhibition efficiency of 97.85% at 750 ppm. However, beyond this concentration, a decline in efficiency is observed.

Table 1. Electrochemical parameters in the absence and presence of different concentrations of Arum italicum extracts at 25°C

C (ppm)	E_{corr} (mV)	I_{corr} (mA.cm^{-2})	b_a (mV)	b_c (mV)	E%
Blank	-482.4	1.224	117.3	-236.4	/
100	-510	0.0808	160	-110.1	93.37
200	-485.4	0.0748	120.1	-136.3	93.87
400	-499.8	0.0723	93	-68.9	94.07
600	-466.889	0.03925	84.7	-108.2	96.8
750	-425.85	0.02615	66.2	-148.0	97.85
800	-400.82	45.66	54.4	-226.4	96.26

The addition of the extract to the corrosive environment modifies the Tafel slope values, suggesting that both anodic and cathodic reactions are affected. The extract also causes a positive shift in the corrosion potential. According to Ferreira *et al*. (2004) and Li *et al*. (2009), a corrosion potential shift greater than 85 mV compared to the blank indicates that the inhibitor can be classified as either anodic or cathodic. In this study, however, the potential shift is less than 85 mV, indicating that the extract acts as a mixed type inhibitor.

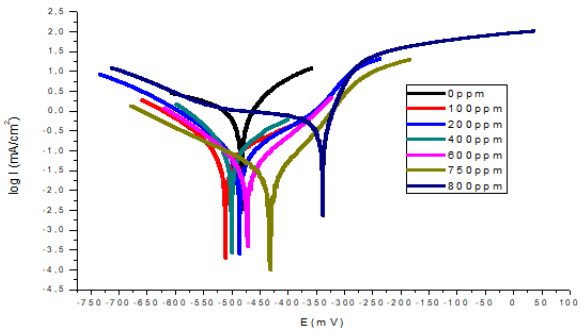

Figure 4. The polarization curves of carbon steel (Fe-C) in 1M HCl in the absence and presence of different concentrations of arum italicum extracts at 25°C

3.2.2. Electrochemical impedance spectroscopy

Electrochemical impedance is an essential technique for studying corrosion and adsorption phenomena, providing valuable insights into the mechanisms at play (Macdonald *et al*., 1992). This method was used to further explore the corrosion and inhibition processes of carbon steel in a 1M HCl environment. Impedance and Bode plots, shown in **Figure 5**, illustrate the behavior in the absence and presence of various concentrations of Arum italicum extract at 298 K.

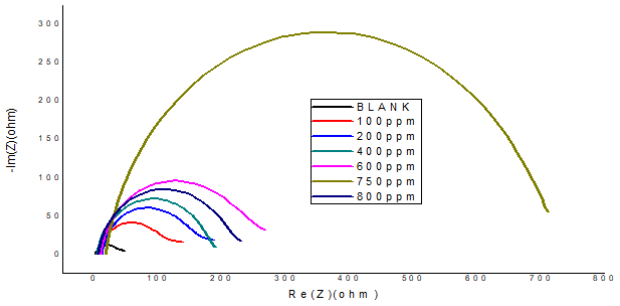

Figure 5. Nyquist diagrams without and with different concentrations of Arum italicum extracts at 25°C

The results reveal that increasing the extract concentration leads to larger semi-circular capacitive loops, which are associated with changes in double-layer capacitance and charge transfer resistance (Rct). A single time constant is observed, likely due to frequency dispersion of the interfacial impedance. The equivalent circuit modeling the electrochemical interface response is shown in **Figure 6**.

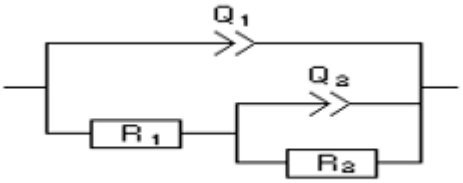

Figure 6. The equivalent circuit simulates the impedance data for steel without and with different extract concentrations at 25°C

The charge transfer resistance (Rt) value measured in the absence of an inhibitor suggests significant steel dissolution during the initial hours of immersion, typically due to a conductive layer of corrosion products (Depenyou *et al*. 2008). As the concentration of the extract increases, there is a corresponding increase in charge transfer resistance (Rtc) and a decrease in double-layer capacitance (Cdl), reaching optimal performance at 750 ppm. These variations in electrochemical parameters are detailed in **Table 2**, highlighting the effectiveness of the extract as an inhibitor. This behavior is attributed to the formation of a protective film on the metal surface, enhancing the film's protective properties, as reflected by the enlargement of the loop sizes in the impedance diagram. The reduction in Q may be linked to a decrease in the dielectric constant and/or an increase in double layer thickness, suggesting that the inhibitor reduces the double-layer thickness and alters the oxide layer, thereby lowering the Q value (Depenyou *et al*. 2008; Mu *et al*. 2005). Calculations indicate a maximum inhibition efficiency of 97.21% at a concentration of 400 ppm of the extract.

Table 2. Electrochemical impedance parameters in the absence and presence of different concentrations of Arum italicum extracts at 25°C

C (ppm)	$R_1(\Omega.cm^2)$	$Q_1(\mu F.10^3)$	a_1	$R_2(\Omega.cm^2)$	a_2	$Q_2(\mu F.10^3)$	E%
Blank	1.44	0.012	0.106	52.93	0.812	0.301	/
100	8.015	6.198	0.084	750	0.9271	0.110	90.4
200	11.76	4.336	0.069	850	0.925	0.10	93.77
400	3.53	4.31	0.022	1000	0.98	0.18	94.70
600	9.164	2.92	0.065	1250	0.909	0.16	95.76
750	17.46	0.872	0.017	1900	0.895	0.134	97.21
800	5.28	3.44	0.039	1050	0.895	0.17	94.95

3.2.3. Adsorption Isotherms

The inhibition of metal corrosion by organic compounds is primarily attributed to their adsorption onto the metal surface. Adsorption isotherms are essential for understanding the adsorption behavior of these compounds on the metal. To construct an isotherm, it is necessary to measure the surface coverage of the metal as a function of the inhibitor concentration (Alsabagh *et al*. 2006).

$$\theta = \frac{bC_{inh}}{1+bC_{inh}} \left(\text{Isotherme de Langmuir}\right) \quad (3)$$

$$\exp(-2a\theta) = KC_{inh} \text{ (Isotherme de Temkin)} \quad (4)$$

$$\left(\frac{\theta}{1+\theta}\right)\exp(2a\theta) = KC_{inh} \text{ (Isotherme de Frumkin)} \quad (5)$$

In this study, various adsorption isotherms were evaluated to identify the most suitable model for describing the adsorption process. The relationship between surface coverage (θ) and inhibitor concentration (Cinh) is defined by several equations that include parameters such as the adsorption coefficient (b), equilibrium constant (K), and interaction constant (a) among adsorbed particles.

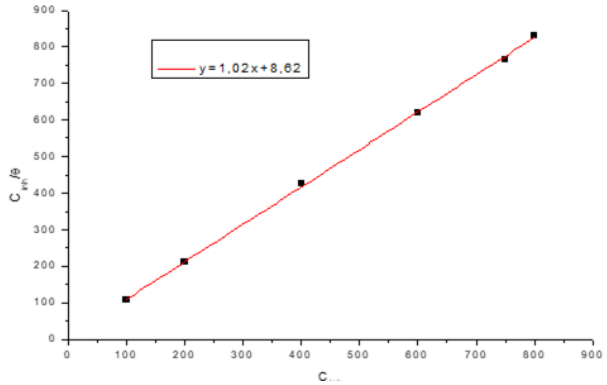

Figure 7. Langmuir adsorption isotherm for steel with different concentrations of Arum italicum extracts at 25°C

The analysis based on the correlation coefficient (R^2) values revealed that the Langmuir isotherm model provided the best fit (**Figure 7**), with an R^2 value of 0.99. The variation in the slope of the curve can be attributed to the interactions either attractive or repulsive between the molecules adsorbed on the metal surface (Deng *et al*. 2011).

The equilibrium constant for adsorption (K_{ads}) is related to the standard free energy of adsorption (ΔG^0_{ads}) by the following equation:

$$K_{ads} = \frac{1}{55.5}\exp\left(\frac{-\Delta G^0_{ads}}{RT}\right) \quad (6)$$

where R is the ideal gas constant, T is the temperature, and 55.5 is the molar concentration of water in the solution.

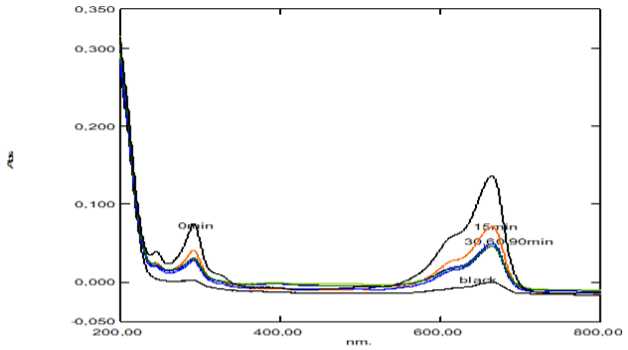

Figure 8. The Equilibrium time curve

After performing the calculations, a ΔG^0_{ads} value of -9.9024 kJ/mol was obtained. The negative value of ΔG^0_{ads} indicates that the adsorption of inhibitor molecules on the metal surface is a spontaneous process. Research suggests that when ΔG^0_{ads} is close to –20 kJ/mol, the adsorption is primarily driven by electrostatic interactions between charged molecules and the metal surface (physisorption). Conversely, when ΔG^0_{ads} approaches –40 kJ/mol, the adsorption involves the formation of covalent bonds between the inhibitor molecules and the metal surface (chemisorption) (Alsabagh *et al*. 2006; Deng *et al*. 2011). In this study, the calculated ΔG^0_{ads} values are slightly less negative than −20 kJ/mol, suggesting that the adsorption process is primarily governed by physisorption.

3.3. Photocatalytic activity of synthesized Ag NPs/Al

3.3.1. Equilibrium time curve

Figure 8 shows the equilibrium time curve. Before irradiation, the system is kept in a dark room to optimize the adsorption/desorption equilibrium time, which was found to be reached within 30 minutes. Once this equilibrium is established, the photocatalytic process can begin. The photocatalytic performance of the synthesized material was evaluated by monitoring the degradation of methylene blue (MB) in aqueous solutions exposed to visible light.

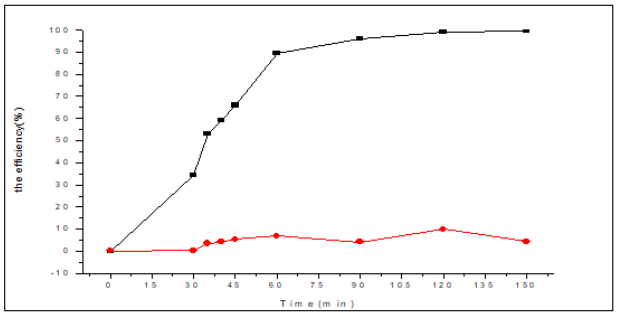

Figure 9. MB degradation rate with and without atalyst

The efficiency of photodegradation is calculated using a specific equation (Eq.7). **Figure 8** depicts the progression of degradation activity over time, both in the absence and presence of the green catalyst.

$$efficiencydegradation(\%) = \frac{C_0 - C}{C_0} \times 100 \quad (7)$$

The efficiency of photodegradation is calculated using a specific equation. **Figure 9** illustrates the progression of degradation activity over time, both in the absence and presence of the green catalyst. The time-dependent absorption spectra for the synthesized photocatalyst are presented in **Figure 6**. A distinct absorption peak at 664 nm, corresponding to the MB dye, diminishes as the irradiation time increases (0, 10, 20, 30, and 60 minutes) in the presence of Ag NPs. The Ag NPs demonstrated a photocatalytic degradation efficiency of approximately 98% after 150 minutes of sunlight exposure. These findings strongly suggest that Ag NPs exhibit significant photocatalytic activity when exposed to sunlight,

indicating that sunlight greatly enhances the photocatalytic process of the Ag NPs.

3.3.2. Antimicrobial activity

The results of the antimicrobial tests, as shown in **Table 3**, indicate substantial inhibition zones for varying concentrations of the tested substance against *E. coli*, *S. aureus*, and *P. aeruginosa*. The maximum inhibition zones were observed to be 20.33 mm for *E. coli*, 20.75 mm for *S. aureus*, and 20.66 mm for *P. aeruginosa*, all at a concentration of 2048 µg/mL (**Figure 10**). These findings demonstrate a dose-dependent response, with antimicrobial activity increasing as the concentration of the substance rises. The silver nanoparticles proved to be effective against both gram-positive and gram-negative bacteria, underscoring their antimicrobial capabilities. Moreover, a decrease in microbial growth was noted with higher nanoparticle concentrations, aligning with previously reported studies (Singhal *et al*. 2011). These encouraging results indicate a potent antimicrobial potential of the substance, outperforming the results obtained in other studies on the antimicrobial effectiveness of Ag NPs synthesized using *Arum italicum* (Seçkin *et al*. 2022).

Table 3. Antimicrobial activity results

Bacteria	Inhibition diameter (mm)						
	Concentration						
	2048 µg mL^{-1}	1024 µg mL-1	512 µg mL-1	256 µg mL-1	128 µg mL-1	64 µg mL-1	32 µg mL-1
E. coli	20.33±0.57	18.00±1.09	16.33±0.66	15.00±1.06	13.00±0.35	11.75±0.57	10.75±0.71
S. aureus	20.75±1.06	18.66±1.33	16.75±0.71	14.50±1.21	11.25±0.66	10.75±0.71	9.25±0.35
P.aeruginosa	20.66±1.41	18.75±1.71	17.00±0.89	16.25±1.33	12.00±0.33	11.25±0.71	10±1.06

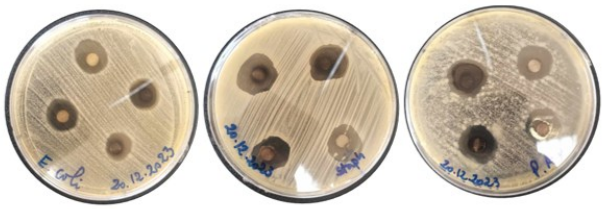

Figure 10. Some images obtained by the disk diffusion method

4. Conclusion

This study on anticorrosion was conducted using electrochemical techniques, including impedance spectroscopy (EIS) and polarization curves, yielding several key findings. The ethanolic extract of Arum italicum proved to be an effective corrosion inhibitor for carbon steel (Fe-C) in a 3% HCl solution, with its effectiveness influenced by both concentration and temperature. The highest inhibition efficiency recorded from the polarization curves was 97.85% at a concentration of 750 ppm, while EIS measurements indicated a similar efficiency of 97.21%. Consistency was observed between the data obtained from polarization curves and EIS measurements, confirming the reliability of the results. Polarization studies further verified that the Arum italicum extract functions as a mixed-type inhibitor. additionally, the green synthesis of silver nanoparticles resulted in a satisfactory product yield. In terms of photocatalytic activity, the degradation of methylene blue (MB) under irradiation demonstrated that approximately 80% of the MB solution was degraded within 60 minutes in the presence of the catalyst, with nearly complete degradation observed after 150 minutes. The antimicrobial activity tests showed significant inhibition zones for various concentrations of the tested substance against *E. coli*, *S. aureus*, and *P. aeruginosa*. The silver nanoparticles were effective against both gram-positive and gram-negative bacteria, underscoring their antimicrobial potential. Moreover, higher concentrations of nanoparticles led to a more pronounced reduction in microbial growth.

Declarations of interest

The authors declare no conflict of interest in this reported work.

Funding declaration

The authors declare no Funding in this publication

Acknowledgement

We gratefully acknowledge the Laboratory Engineer Ladacia Sana for his participation in carrying out my work at the research laboratory level (LGCES), University-20 August-1955-Skikda, Algeria.

References

Ahmad Khan M.S.et al. (2019). Ahmad, Chapter 1 - Herbal Medicine: Current Trends and Future Prospects, in *New Look to Phytomedicine*, M.S. Ahmad Khan I. Ahmad *et al*. Chattopadhyay, Éd., Academic Press, 3–13. doi: 10.1016/B978-0-12-814619-4.00001-X.

Ahmed S.F. *et al.* (2022). Green approaches in synthesising nanomaterials for environmental nanobioremediation: Technological advancements, applications, benefits and challenges, *Environ. Res.*, **204**, 111967, doi: 10.1016/j.envres.2021.111967.

Al-Amiery A., Wan Isahak W.N.R., Al-Azzawi K. (2024). Sustainable corrosion Inhibitors: A key step towards environmentally responsible corrosion control, *Ain Shams Eng. J.*, **15**(5), 102672, doi: 10.1016/j.asej.2024.102672.

Alsabagh A.M., Migahed M.A., *et al*. (2006). Awad, Reactivity of polyester aliphatic amine surfactants as corrosion inhibitors for carbon steel in formation water (deep well water), *Corros. Sci.*, **48**(4), 813–828, doi: 10.1016/j.corsci.2005.04.009.

Barrett B. *et al*. (2001). Kieffer, Medicinal Plants, Science, and Health Care, *J. Herbs Spices Med. Plants*, **8**, no2–3, 1–36, doi: 10.1300/J044v08n02_01.

Behpour M., Ghoreishi S M., Soltani N., Salavati-Niasari M., Hamadanian M., *et al*. (2008). Gandomi, Electrochemical and theoretical investigation on the corrosion inhibition of mild steel by thiosalicylaldehyde derivatives in hydrochloric acid solution, *Corros. Sci.*, **50**(8), 2172–2181, doi: 10.1016/j.corsci.2008.06.020.

Bouzana A., Zohra C., Becheker I., Sakhraoui N., Bouzenad N. *et al*. (2023). Chawki, Phytochemical analysis by LC MS/MS and in vitro antioxidant activity of the Algerian endemic plant Dianthus sylvestris subsp. aristidis (Batt.) Greuter & Burdet, *Glob. NEST J.*, **25**, 113–119, doi: 10.30955/gnj.005047.

Bouzenad N. *et al.* (2024). Development of Bioplastic Films from Sargassum muticum Alginate: Properties and Applications in Food Packaging, *Iran. J. Chem. Chem. Eng.*, doi: 10.30492/ijcce.2024.2023449.6460.

Bouzenad N. *et al.* (2024). Exploring Bioactive Components and Assessing Antioxidant and Antibacterial Activities in Five Seaweed Extracts from the Northeastern Coast of Algeria, *Mar. Drugs*, **22**(6), Art. no 6, doi: 10.3390/md22060273.

Calabrese G. and Gaetano T.N. (2012). *Study on biodiversity in century-old olive groves*.

Deng S., Li X., *et al*. (2011). Fu, Two pyrazine derivatives as inhibitors of the cold rolled steel corrosion in hydrochloric acid solution, *Corros. Sci.*, 53(2), 822–828, févr. doi: 10.1016/j.corsci.2010.11.019.

Depenyou F., Doubla A., Laminsi S., Moussa D., Brisset J.L. *et al*. (2008). Le Breton, Corrosion resistance of AISI 1018 carbon steel in NaCl solution by plasma-chemical formation of a barrier layer, *Corros. Sci.*, vol. 50(5), 1422–1432, doi: 10.1016/j.corsci.2007.12.011.

Ferkous H., Dilemi A., Abdennouri A. and Malha S.I.R. (2023). Study of the electrochemical behavior of Al-Zn-In based sacrificial anodes in sea water, *Synthèse Rev. Sci. Technol.*, **29**(1), 36–43.

Ferreira E.S., Giacomelli C., Giacomelli F.C. *et al*. (2004). Spinelli, Evaluation of the inhibitor effect of l-ascorbic acid on the corrosion of mild steel, *Mater. Chem. Phys.*, 83(1), 129–134, doi: 10.1016/j.matchemphys.2003.09.020.

Govindaraju K., Basha S.K., Kumar V.G. *et al*. (2008). Singaravelu, Silver, gold and bimetallic nanoparticles production using single-cell protein (Spirulina platensis) Geitler, *J. Mater. Sci.*, **43**(15), 5115–5122, doi: 10.1007/s10853-008-2745-4.

Haneefa M.M. (2017). Green Synthesis Characterization and Antimicrobial Activity Evaluation of Manganese Oxide Nanoparticles and Comparative Studies with Salicylalchitosan Functionalized Nanoform, *Asian J. Pharm. AJP*, **11**, no 01, Art. no 01, doi: 10.22377/ajp.v11i01.1045.

Harish V. *et al.* (2022). Review on Nanoparticles and Nanostructured Materials: Bioimaging, Biosensing, Drug Delivery, Tissue Engineering, Antimicrobial, and Agro-Food Applications, *Nanomaterials*, **12**(3), Art. 3, doi: 10.3390/nano12030457.

Himeur T. *et al.* (2024). Unlocking the power of *Inula Viscosa* essential oil: A green solution for corrosion inhibition in XC48 steel within acidic environments, *Process Saf. Environ. Prot.*, vol. **187**, 1422–1445, doi: 10.1016/j.psep.2024.05.061.

Hublikar L.V. *et al.* (2021). Biogenesis of Silver Nanoparticles and Its Multifunctional Anti-Corrosion and Anticancer Studies, *Coatings*, 11(10), 10, doi: 10.3390/coatings11101215.

Imchen P., Ziekhrü M., Zhimomi B.K. *et al*. (2022). Phucho, Biosynthesis of silver nanoparticles using the extract of *Alpinia galanga* rhizome and *Rhus semialata* fruit and their antibacterial activity, *Inorg. Chem. Commun.*, **142**, 109599, doi: 10.1016/j.inoche.2022.109599.

Imchen P., Ziekhrü M., Zhimomi B.K. *et al*. (2022). Phucho, Biosynthesis of silver nanoparticles using the extract of *Alpinia galanga* rhizome and *Rhus semialata* fruit and their antibacterial activity, *Inorg. Chem. Commun.*, **142**, 109599, doi: 10.1016/j.inoche.2022.109599.

Kavitha V., Mahalingam P., Jeyanthinath M. et N. Sethupathi N. Optical and structural properties of tungsten-doped barium strontium titanate, *Mater. Today Proc.*, **23**, 1215, doi: 10.1016/j.matpr.2019.05.351.

Kozuharova E. *et al.* (2023). Bioactive Compounds and Biological Activities of Arum L., in *Bioactive Compounds in the Storage Organs of Plants*, H. N. Murthy, K. Y. Paek, et S.-Y. Park, Éd., Cham: Springer Nature Switzerland, 1–34. doi: 10.1007/978-3-031-29006-0_6-1.

Lengke M.F., Fleet M.E. *et al*. (2007). Southam, Biosynthesis of Silver Nanoparticles by Filamentous Cyanobacteria from a Silver(I) Nitrate Complex, *Langmuir*, **23**(5), 2694–2699, févr. 2007, doi: 10.1021/la0613124.

Li W., He Q., Zhang S., Pei C. *et al*. (2008). Hou, Some new triazole derivatives as inhibitors for mild steel corrosion in acidic medium, *J. Appl. Electrochem.*, 38(3), 289–295, mars 2008, doi: 10.1007/s10800-007-9437-7.

Liu H., Wang M., Zhang X., Ma J. *et al*. (2018). Lu High efficient photocatalytic hydrogen evolution from formaldehyde over sensitized Ag@Ag-Pd alloy catalyst under visible light irradiation, *Appl. Catal. B Environ.*, **237**, 563–573, déc. 2018, doi: 10.1016/j.apcatb.2018.06.028.

Macdonald J.R. (1992). Impedance spectroscopy, *Ann. Biomed. Eng.*, 20(3), 289–305, doi: 10.1007/BF02368532.

Medhi R., Marquez M.D. et Lee T.R. (2020). Visible-Light-Active Doped Metal Oxide Nanoparticles: Review of their Synthesis, Properties, and Applications, *ACS Appl. Nano Mater.*, **3**(7), no 7, 61566185, doi: 10.1021/acsanm.0c01035.

Meeuse B.J.D., Arum: En. Arum; Fr. Gouet; Ge. Aronstab, in *Handbook of Flowering*, CRC Press, 1989.

Meydan I., Seckin H., Burhan H., Gür T., Tanhaei B. *et al.* (2022). Sen, *Arum italicum* mediated silver nanoparticles: Synthesis and investigation of some biochemical parameters, *Environ. Res.*, **204**, 112347, doi: 10.1016/j.envres.2021.112347.

Mu G., Li X., *et al*. (2005). Liu, Synergistic inhibition between tween 60 and NaCl on the corrosion of cold rolled steel in 0.5 M sulfuric acid, *Corros. Sci.*, **47**(8), 1932–1952, doi: 10.1016/j.corsci.2004.09.020.

Nair G.M., Sajini T., et B. (2022). Mathew, Advanced green approaches for metal and metal oxide nanoparticles synthesis and their environmental applications, *Talanta Open*, **5**, 100080, doi: 10.1016/j.talo.2021.100080.

Ouali I.E. *et al.* (2010). Thermodynamic characterisation of steel corrosion in HCl in the presence of 2–phenylthieno (3, 2-b) quinoxaline

Qin H. *et al.* (2019). Effects of Ag nanoparticles on the visible-light-driven photocatalytic properties of Cu2O nanocubes, *Mater. Chem. Phys.*, **232**, 240–245, doi: 10.1016/j.matchemphys.2019.04.081.

Rasool A., Sri S., Zulfajri M. *et al*. (2024). Sri Herwahyu Krismastuti, Nature inspired nanomaterials, advancements in green synthesis for biological sustainability, *Inorg. Chem. Commun.*, **169**, 112954, doi: 10.1016/j.inoche.2024.112954.

Rautaray D., Ahmad A., *et al*. (2003). Sastry, Biosynthesis of CaCO3 Crystals of Complex Morphology Using a Fungus and an Actinomycete, *J. Am. Chem. Soc.*, **125**(48), 14656–14657, doi: 10.1021/ja0374877.

Rechek H. *et al.* (2023). A Comparative Analysis between the Phenolic Content, Key Enzyme Inhibitory Potential, and Cytotoxic Activity of Arum italicum Miller in Two Different Organs, *Int. J. Plant Biol.* **14**(2), Art no 2, doi: 10.3390/ijpb14020041.

Rizi A. *et al.* (2023). Sustainable and Green Corrosion Inhibition of Mild Steel: Insights from Electrochemical and Computational Approaches, *ACS Omega*, **8**(49), 47224–47238, doi: 10.1021/acsomega.3c06548.

Şafak S., Duran B., Yurt A. *et al*. (2012). Türkoğlu, Schiff bases as corrosion inhibitor for aluminium in HCl solution, *Corros. Sci.*, **54**, 251–259, doi: 10.1016/j.corsci.2011.09.026.

Sanna C., Maxia A., Fenu G., *et al*. (2020). So Uncommon and so Singular, but Underexplored: An Updated Overview on Ethnobotanical Uses, Biological Properties and Phytoconstituents of Sardinian Endemic Plants, *Plants*, **9**(8), Art. no 8, doi: 10.3390/plants9080958.

Seçkin H. Meydan et I. (2022). Synthesis and characterization of *Sophora alopecuroides* L. green synthesized of Ag nanoparticles for the antioxidant, antimicrobial and DNA damage prevention activity, *Braz. J. Pharm. Sci.*, **58**, 20992, déc. 2022, doi: 10.1590/s2175-97902022e20992.

Shikov A.N., Pozharitskaya O.N., Makarov V.G., Wagner H., Verpoorte R. *et al*. (2014). Heinrich, Medicinal Plants of the Pharmacopoeia; their history and applications, *J. Ethnopharmacol.*, **154**(3), 481–536, doi: 10.1016/j.jep.2014.04.007.

Shyam A., Chandran S., George B. *et al*. (2021). Plant mediated synthesis of AgNPs and its applications: an overview, *Inorg. Nano-Met. Chem.*, **51**(12), 1646–1662, doi: 10.1080/24701556.2020.1852254.

Singh S. *et al.* (2024). Sustainable Synthesis of Novel Green-Based Nanoparticles for Therapeutic Interventions and Environmental Remediation, *ACS Synth. Biol.*, **13**(7), 1994–2007, doi: 10.1021/acssynbio.4c00206.

Singhal G., Bhavesh R., Kasariya K., Sharma A.R. Singh R.P. *et al*. (2011). Biosynthesis of silver nanoparticles using Ocimum sanctum (Tulsi) leaf extract and screening its antimicrobial activity, *J. Nanoparticle Res.*, 13(7), 2981–2988, doi: 10.1007/s11051-010-0193-y.

Tehri N., Vashishth A., Gahlaut A. *et al*. (2022). Hooda, Biosynthesis, antimicrobial spectra and applications of silver nanoparticles: current progress and future prospects, *Inorg. Nano-Met. Chem.*, **52**(1), 1–19, doi: 10.1080/24701556.2020.1862212.

Zhang B., He C., Chen X., Tian Z. *et al*. (2015). Li, The synergistic effect of polyamidoamine dendrimers and sodium silicate on the corrosion of carbon steel in soft water, *Corros. Sci.*, vol. **90**, 585–596, doi: 10.1016/j.corsci.2014.10.054.

Zouied D., Zouaoui E., Dob K., Chikha O. *et al.* (2022). Fadhli, Antioxidant activity of the strawberry plant extract and its inhibitory efficiency against carbon steel corrosion in 3% NaCl solution, *Curr. Top. Electrochem.*, **24**, 37–50.